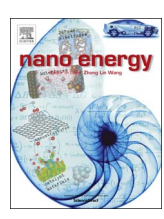


Contents lists available at ScienceDirect

Nano Energy

journal homepage: www.elsevier.com/locate/nanoen



Full paper

A spring-based resonance coupling for hugely enhancing the performance of triboelectric nanogenerators for harvesting low-frequency vibration energy



Changsheng Wu^{a,1}, Ruiyuan Liu^{a,1}, Jie Wang^a, Yunlong Zi^a, Long Lin^a, Zhong Lin Wang^{a,b,c,*}

- ^a School of Materials Science and Engineering, Georgia Institute of Technology, Atlanta, GA 30332-0245, USA
- ^b Beijing Institute of Nanoenergy and Nanosystems, Chinese Academy of Sciences, PR China
- ^c National Center for Nanoscience and Technology (NCNST), Beijing 100083, PR China

ARTICLE INFO

Keywords: Triboelectric nanogenerators Mechanical amplifier Vibration energy Resonance coupling

ABSTRACT

Low-frequency vibration is a ubiquitous energy that exists almost everywhere, but a high efficient harvesting of which remains challenging. Recently developed triboelectric nanogenerator (TENG) provides a promising alternative approach to conventional electromagnetic and piezoelectric generators, with the advantage of low cost and high output voltage. In this work, a mechanical spring-based amplifier with the ability of amplifying both the vibration frequency and amplitude is integrated with TENG to improve its low-frequency performance by up to 10 times. A new scheme for evaluating TENG using the average output power is proposed and the process of choosing an appropriate time interval for analysis is demonstrated. It takes into account the temporal variation in electrical output and offers a more accurate and convincing evaluation of TENG's performance in practical working environment compared to previously used instantaneous power. This work serves as an important progress for the future development and standardization of TENG, especially for harvesting low-frequency vibration energy as well as a great prospect of blue energy.

1. Introduction

Triboelectric nanogenerator (TENG) has emerged as a promising technology for harvesting mechanical energy from the environment recently [1-4]. TENG relies on common phenomena, the triboelectric effect and electrostatic induction, and uses the electrostatic charges created on the surfaces of two dissimilar materials to induce potential change and drive electrons in the electrodes to flow as the distance between oppositely charged surfaces is changed by mechanical motions. Based on such a principle, four different modes including vertical contact-separation, lateral sliding, single-electrode and freestanding triboelectric-layer, have been invented to meet the requirements of various application scenarios. It has been demonstrated to effectively harvest energy of various forms, ranging from human motions like walking to natural resources like wind and ocean waves [5-10]. It can also be used as a self-powered sensor for actively detecting the static and dynamic processes arising from mechanical agitation using the voltage and current output signals [11,12].

Conventionally, the ambient mechanical energy is converted into electricity using electromagnetic generator (EMG). The fundamental operating principle of EMG is Faraday's law of induction, and the technology maturity has enabled its wide application in both small-

scale devices like RF powered tags and large-scale facilities like wind turbines and water dams [13-15]. However, its nature of linear relationship between output voltage/current and operating frequency greatly limits its effectiveness at low frequency (< 5 Hz) [16]. The effective output power obtained at low frequency could barely drive any electronics that has a threshold operation voltage [17-19]. In contrast, the output voltage of TENG is independent of frequency and remains in the range of $10-100~\rm V$ depending on materials and structure design, resulting in a much slower declining rate of power after power management [20-22]. Considering that most ambient mechanical energy is at low frequency, therefore, TENG has a great potential in outperforming EMG when it comes to scavenging energy from irregular human motions for powering small electronics or infrequent ocean waves for large-scale blue energy.

However, the current design of TENG is most effective for harvesting the instantaneous mechanical impact energy at the moment when the mechanical stimulation occurs, while a large portion of impact potential energy is dissipated due to the low triggering frequency. One approach is to use a spring structure to store the mechanical kinetic energy and potential energy and convert a low frequency triggering to a higher frequency oscillation, resulting in high average output power. In this work, a mechanical spring-based amplifier with the ability of

^{*} Corresponding author at: School of Materials Science and Engineering, Georgia Institute of Technology, Atlanta, GA 30332-0245, USA. E-mail address: zlwang@gatech.edu (Z.L. Wang).

¹ C.W. and R.L. contributed equally to this work.

amplifying both the vibration frequency and amplitude is integrated with TENG to improve its low-frequency performance. The features of amplified frequency and displacement enable the device to have a higher output power at low frequency and the performance boost can be up to 10 times in comparison to the conventional reference TENG that does not have the amplifier. The mechanical amplifier-assisted TENG (MA-TENG) also has a lower minimum working frequency (2.5 Hz) compared to its counterpart. This work introduces a fundamental concept of mechanical amplifier to the emerging field of TENG for largely enhancing its performance in harvesting low-frequency vibration energy, and thus is of great importance for future progress towards the highly anticipated prospect of large-scale blue energy. The proposed methodology of using average output power for quantitative comparison of MA-TENG and conventional reference TENG is capable of capturing the performance difference triggered by mechanical amplification (e.g. frequency upscaling), which is impossible for previously used instantaneous power that does not take into account the temporal variation in electrical output. Therefore, the method serves as a great scheme for evaluating and standardizing TENG's performance in practical working environment.

2. Device structure

Most conventional TENGs for harvesting vibration energy can be simplified as a single-spring resonator (referred to as SR-TENG below), and work on either contact-separation mode or single-electrode mode. In this work the single-electrode mode was chosen as the study subject but the concept applies to the contact-separation mode as well. A typical single-electrode SR-TENG consists of a single mass (denoted by m_0 , 60.87 g) and a spring for resonant vibration, with one copper film attached on the top base of the device and a PTFE film attached on the vibrating mass m_0 , as illustrated in the left-hand schematic of Fig. 1(a). The PTFE film serves as one triboelectric layer while the copper film functions as the other triboelectric layer as well as an electrode connected to external loads. Fig. 1(b) and (c) present the working mechanism of the single-electrode TENG under short-circuit condition and numerically calculated potential distribution of three typical states under open-circuit condition respectively. At the initial state i, the copper electrode and PTFE film are in contact and there is no current flow or potential difference. Due to different surface electron affinities, however, the electrons will be transferred from the copper electrode surface to the PTFE surface, leaving net positive charges on the electrode surface and net negative charges on the PTFE surface. When the electrode and PTFE film separates (state ii), the resulted charge separation will induce positive potential on the electrode relative to the ground under open-circuit condition, while under short-circuit condition, electrons will be driven from the ground to the electrode. At the maximum separation distance (state iii), the opencircuit potential on the electrode will reach its maximum value. When the distance decreases as the PTFE film moves towards the electrode (state iv), the positive open-circuit potential on the electrode will decrease while electrons will flow from the electrode to the ground under short-circuit condition. Under vertical vibration, the relative distance change between the electrode and the PTFE film is realized by the movement of m_0 , whose upward velocity is obtained by impacting with the bottom base, as illustrated in Fig. 2(a). In the simplest case that m_0 undergoes free fall before impact and the bottom base behaves like the ground, the conservation of momentum requires that velocity of m_0 after impact is equal to

$$v_0' = e_{0,g} v_0 \tag{1}$$

where v_0 is the free-fall velocity and $e_{0,g}$ is the coefficient of restitution between m_0 and the bottom base. In perfect elastic collision, the coefficient of restitution will be 1 and m_0 only changes moving direction without velocity loss.

A mechanical amplifier, as the name suggests, is a mechanical

system used to amplify the magnitude of mechanical quantities such as velocity, frequency, displacement, etc. [23-25]. Its origin can be dated back to the ancient times when levels and gear trains were invented, and it is ubiquitous in our everyday life, with applications ranging from small devices like diaphragms operating at resonating frequency to large systems like automotive drivetrains. With regards to mechanical energy harvesting, various types of frequency upscalers have been adopted and demonstrated to improve the performance of EMG or piezoelectric generators operating at a frequency lower than their resonating frequency [24-26]. Inspired by the frequency-upscaling EMG and the TENG, an MA-TENG was proposed and fabricated to harvest the low-frequency vibration energy more effectively. In MA-TENG, the single mass m_0 in SR-TENG is split into two masses, m_1 (55.91 g) and m_2 (4.28 g) and an additional spring is introduced to achieve resonance coupling, as illustrated in the right-hand schematic of Fig. 1(a). Under vertical vibration, as illustrated in Fig. 2(b), m_1 will gain an upward velocity $e_{1,q}v_0$ after impacting with the bottom base, followed by the collision between m_1 and m_2 . The sequential pairwise collision between the bottom base, m_1 , and m_2 , is capable of transferring kinetic energy from m_1 to m_2 and amplifying the velocity of final mass m_2 when $m_1 > m_2$. This process is also called velocity amplification and can be described by a set of equations using rigid body mechanics [27,28]. As in SR-TENG, the collision between the bottom base and m_1 can be described by

$$v_1 = e_{1,g} v_0 (2)$$

As for the collision between m_1 and m_2 , the first equation is given by the conservation of momentum,

$$m_1 v_1 + m_2 v_2 = m_1 v_1' + m_2 v_2' \tag{3}$$

where v_i and v_i' are the velocity of m_i before and after collision respectively. The kinetic energy loss during collision is accounted for by the coefficient of restitution $e_{2.0}$,

$$e_{2,1} = \frac{v_2' - v_1'}{v_1 - v_2} \tag{4}$$

By combining Eqs. (3) and (4), the velocity of m_2 after impact is solved as

$$v_2' = \frac{m_1 v_1 (1 + e_{2,1}) + (m_2 - m_1 e_{2,1}) v_2}{m_1 + m_2}$$
(5)

By substituting Eq. (2) and $v_2 = -v_0$ into Eq. (5) and reorganizing,

$$v_2' = \left[\frac{(1 + e_{1,g})(1 + e_{2,1})}{1 + m_2/m_1} - 1 \right] v_0 \tag{6}$$

Therefore, the final velocity gain of m_2 with respect to the m_0 after impact is

$$G = \frac{v_2'}{v_0'} = \frac{1}{e_{0,g}} \left[\frac{(1 + e_{1,g})(1 + e_{2,1})}{1 + m_2/m_1} - 1 \right]$$
(7)

In perfect elastic collision, the coefficients of restitution will be 1 and velocity gain is 2.72. The higher velocity of m_2 enables it to travel quicker and higher through the shaft than m_0 , and thus the PTFE film in MA-TENG could be in contact with the top electrode more easily and more frequently as compared to the one in SR-TENG, even when the latter could not reach the top under the same ambient vibration. In other words, the mechanical amplifier is able to act as a frequency amplifier and a displacement amplifier simultaneously in MA-TENG. However, it is important to note that Eqs. (6) and (7) are derived under the strict constraints of sequential pairwise collisions and rigid-body mechanics. In real devices under forced excitation, e.g. external vibration, the collisions take place over a finite time interval especially when springs are involved, and the sequence of impacts may vary. The velocity gain from a collision may even be smaller than 1 due to the change of impact sequence. For example, if m_2 collides with m_1 before the latter hits the base and reverses its downward moving direction, the

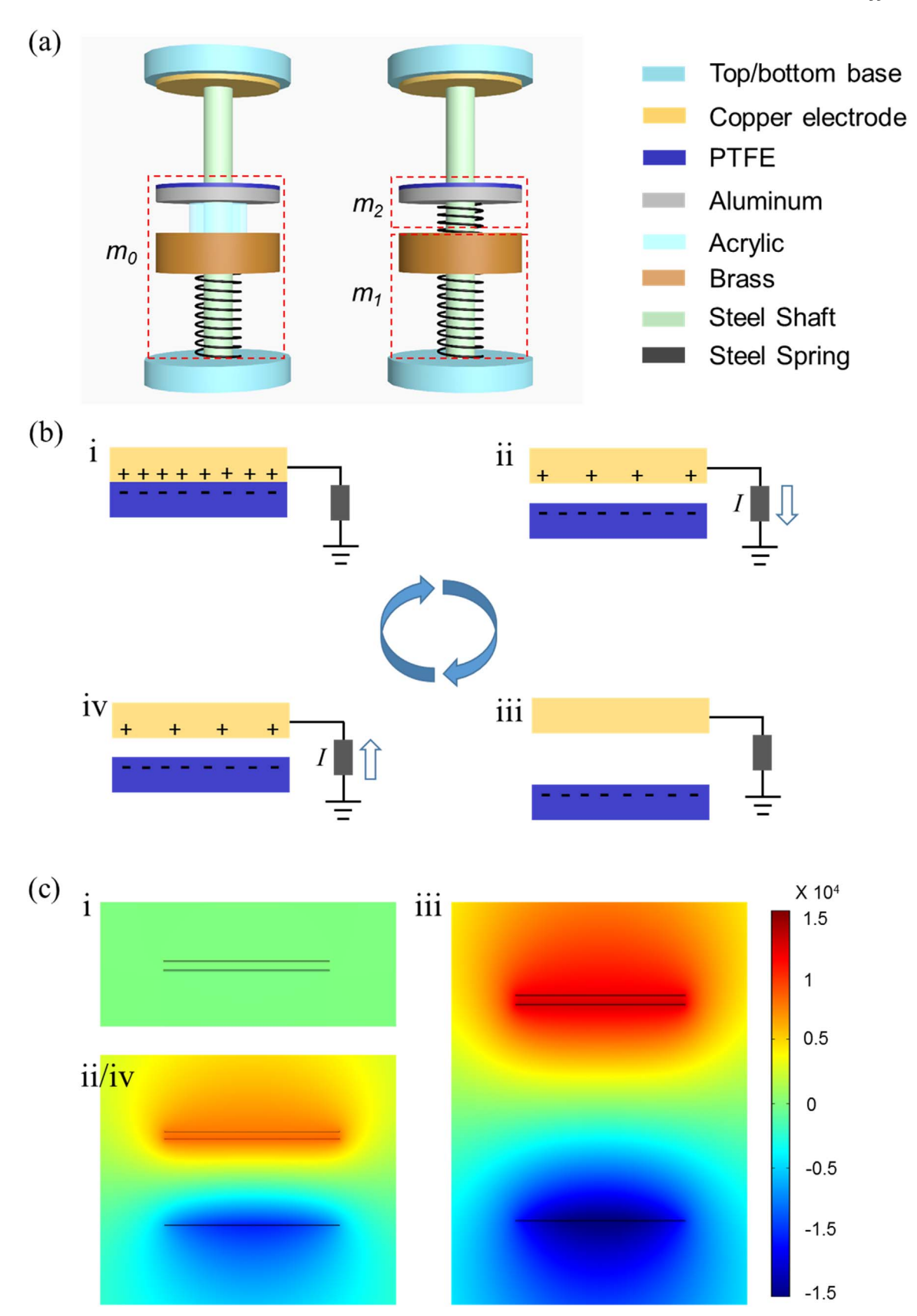


Fig. 1. (a) Device schematic of single-spring resonator based triboelectric nanogenerator (SR-TENG; left) and mechanical amplifier-assisted triboelectric nanogenerator (MA-TENG; right) consisting of two springs. (b) Working mechanism of the MA-TENG under short-circuit condition. (c) Numerical calculations of the potential on TENG electrodes at three typical states, as evaluated by COMSOL.

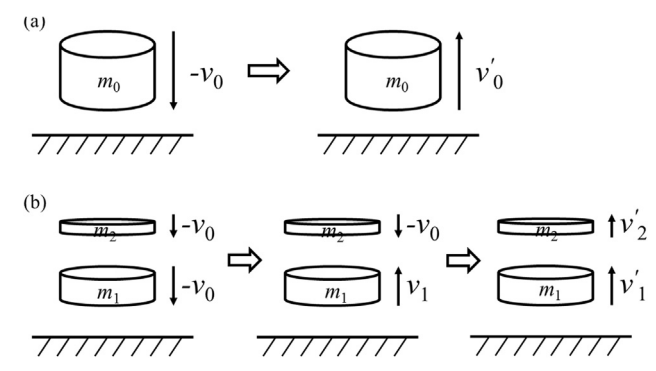


Fig. 2. Schematics of sequential collisions in (a) SR-TENG and (b) MA-TENG.

velocity of m_2 will decrease instead of being amplified. Also, the bottom base, which is also under vibration, acts as an "active ground" rather than a "still ground", and its impact with the m_0 or m_1 may increase or reduce their falling velocity when $e_{i,g} > 1$ or $e_{i,g} < 1$ respectively. With all the above being accounted for, at certain frequencies, the event that the velocity gain of the masses from collision is smaller than 1 has higher chance of occurrence, and thus the electrical output may reach a local minimum.

3. Qualitative comparison of electrical outputs

The performance of SR-TENG and MA-TENG was studied under ambient vibration ranging from 2.5 to 6.0 Hz. Fig. 3(a) and (b) plots their typical short-circuit current at 3.5 Hz, 4.5 Hz and 6.0 Hz frequency respectively, and the outputs at other frequencies are presented in Fig. S2. The results provide a clear qualitative comparison of the electrical outputs of the two devices. At the same ambient vibration

frequency, more current peaks were generated from the MA-TENG, whereas the current peaks correspond to the contact between the PTFE film and the top electrode when the m_0 or m_2 collides with the top base. Fig. 3(c) plots the typical short-circuit current output under ambient vibration of 6.0 Hz over a short time domain of 1 s. It can be observed that the number of peaks from SR-TENG, 6, was exactly the same as the frequency while the number of clearly distinguishable peaks from MA-TENG was at least 10, nearly double of the frequency. Therefore, the output frequency of MA-TENG has been experimentally validated to be higher than that of SR-TENG when they are under the same ambient vibration frequency, which confirms the presence of frequency amplification in MA-TENG. As elaborated above, this amplified output frequency can be attributed to the amplified velocity of m_2 obtained from the collision with m_1 since the frequency of contact increases when the PTFE film moves faster towards the top electrode. Also, the minimal vibration frequency required for achieving contact between the PTFE film and top electrode in MA-TENG (2.5 Hz) is lower than that of SR-TENG (3.5 Hz), which is owing to that the amplified velocity helps the PTFE film reach the top more easily and thus proves the existence of displacement amplification. Another point worth noting is that the average value of short-circuit current peaks of both TENGs increases as the vibration frequency increases from 2.5 to 6.0 Hz. This can be well explained by the equation

$$I = \frac{dQ}{dt} \tag{8}$$

where I is electrical current, Q is transferred charge and t is time. Firstly, when the frequency is higher, the PTFE film on m_0 or m_2 can gain a higher upward velocity, making the time dt shorter; Secondly, when the velocity of m_0 or m_2 is higher, based on the Impulse-Momentum Theorem,

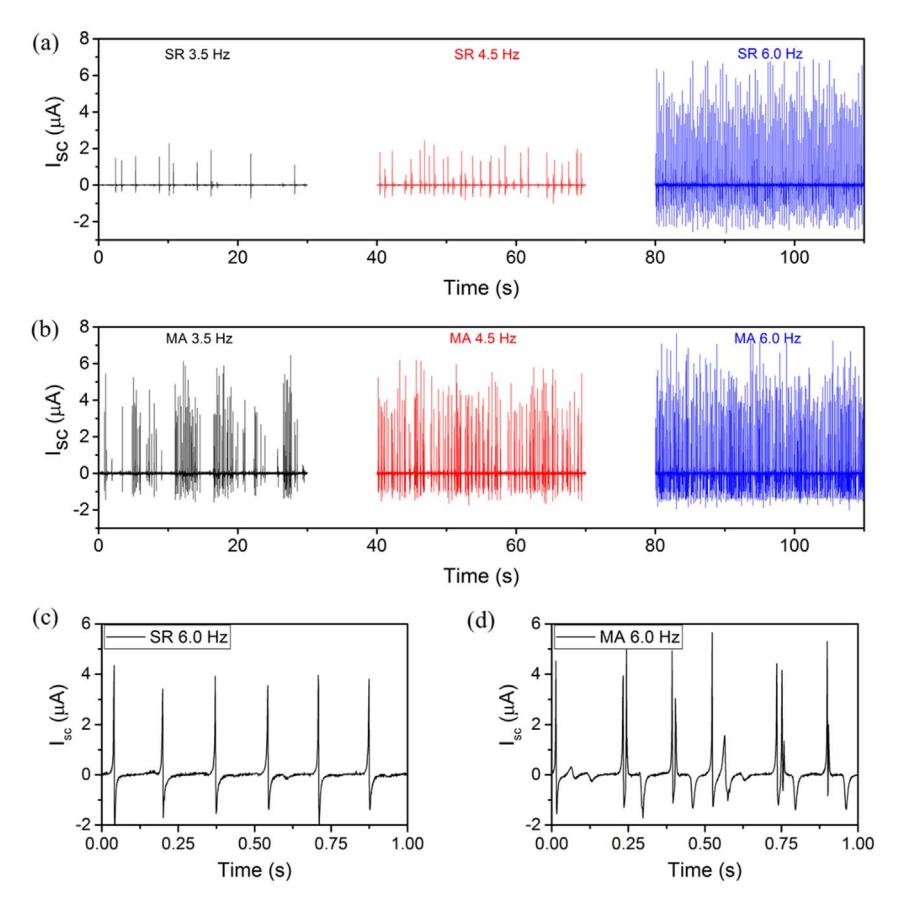


Fig. 3. Typical short-circuit current of (a) MA-TENG and (b) SR-TENG operating at 3.5, 4.5 and 6.0 Hz vibration frequency over a 30-second time domain. (c) & (d) Zoom-in comparison of short-circuit current by the two configurations at 6.0 Hz in a short 1-second time domain.

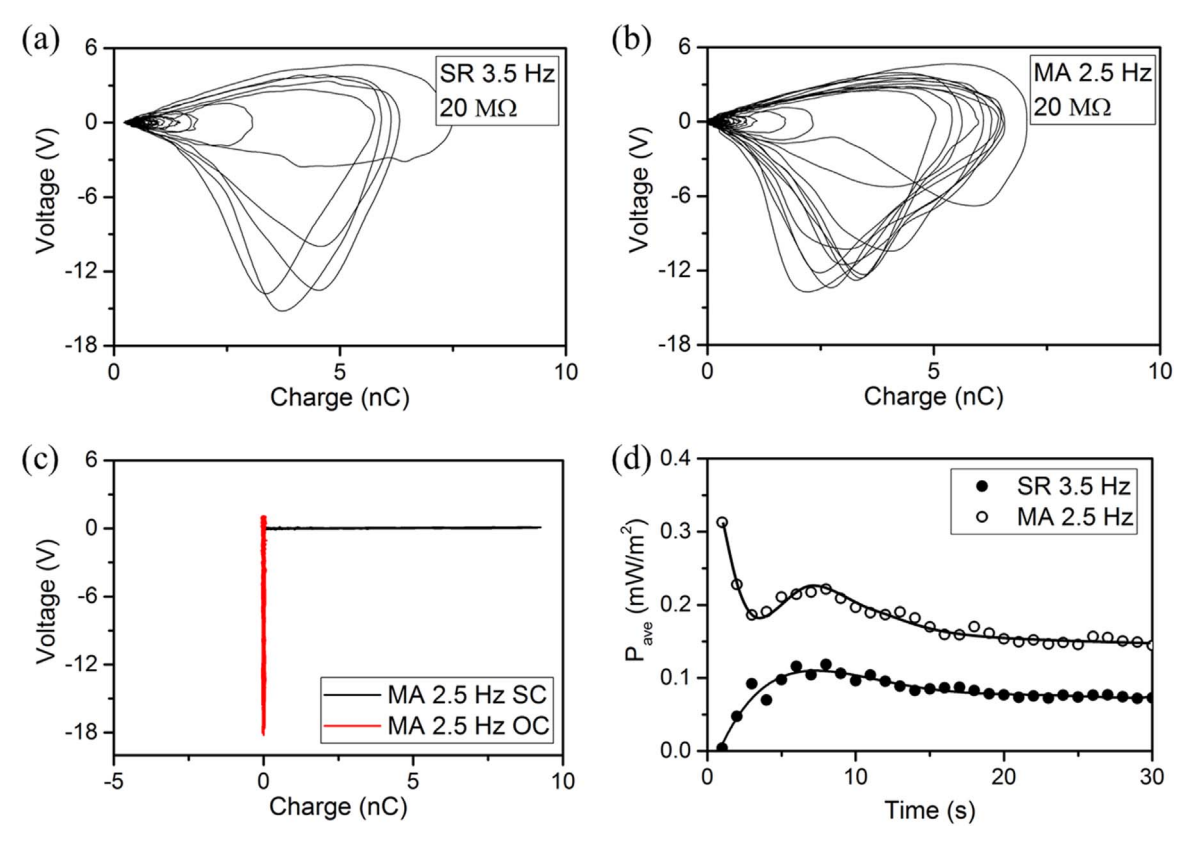


Fig. 4. Typical V-Q characteristics of (a) SR-TENG at 3.5 Hz vibration, (b) MA-TENG at 2.5 Hz vibration for 5 s when connected to the matched load resistance of 20 MΩ. (c) The short-circuit and open-circuit V-Q plots of the MA-TENG at 2.5 Hz vibration. (d) Convergence study of the average output power over different length of time intervals for SR-TENG at 3.5 Hz vibration and MA-TENG at 2.5 Hz vibration.

$$Fdt = mdv (9)$$

the impact force between the PTFE film and the top electrode will be larger, resulting in more intimate contact. The more intimate contact can enhance the generation of triboelectric charges and thus brings about higher dQ. With shorter dt and higher dQ, the current would be higher as the ambient frequency increases.

4. Quantitative comparison using average output power

Although the short-circuit current has provided a strong, qualitative comparison of the two TENGs, power remains one of the most intuitive and effective measures to quantitatively evaluate the performance of electricity generation devices. Most previous work about TENGs [29-32] used the concept of maximum instantaneous power to represent the strength of their output, however, instantaneous power is prone to overestimate the performance without the consideration of temporal variation. Meanwhile, the average power, albeit requiring more computational efforts to calculate, provides a more accurate account of the actual work that can be achieved from a generator in a practical time interval. It is given by

$$P_{ave} = \int V I dt / \Delta t \tag{10}$$

where V is the voltage across the applied load, I is the current flowing through it, and Δt is the length of selected time interval. Recently Zi et~al. proposed a set of figure of merits for standardizing TENGs [33] as well as a rationally designed charging cycle using TENGs [34], both of which emphasized the significance of voltage V and transferred charge Q, or V-Q plot, on the evaluation and maximization of TENG performance. Therefore, it makes sense to expressing the power equation using V and Q by substituting Idt with dQ,

$$P_{ave} = \int V dQ / \Delta t \tag{11}$$

According to both Eqs. (10) and (11), the length of time interval Δt is a very critical parameter that would greatly affect the validity of calculated average power as well as the amount of required computational efforts. If Δt is too short, the interval would not be adequate to give a reliable estimate of the long-term performance of the TENG; if it is too long, the process of experimental measurement and data analysis would be inefficient. The most straightforward choice of Δt is the period of the electrical output. However, as seen in Fig. 3, the outputs of both SR-TENG and MA-TENG under ambient vibration are not periodic from cycle to cycle. Fig. 4(a) and (b) plot typical V-Q characteristics of SR-TENG under 3.5 Hz vibration and MA-TENG under 2.5 Hz vibration when connected to a 20 $M\Omega$ external resistor over a 5-seconds interval respectively. The results clearly show that the work done per cycle (the area of a cycle in the plots) varies greatly and it would be insufficient to randomly chose a cycle length for Δt . The validity of the measured V-Q plot is proven by Fig. 4(c), which presents the shortcircuit and open-circuit V-Q plots of the MA-TENG under 2.5 Hz vibration. In open-circuit condition, the transferred charge would be zero and the plot is nearly a vertical line at Q=0; while in short-circuit condition, the output voltage would be zero and the plot is nearly a horizontal line at V=0. To determine the proper length of time interval for calculating the average power, a convergence study by averaging the electrical work done over different time intervals was proposed and conducted, with results shown in Fig. 4(d). For both SR-TENG under 3.5 Hz vibration and MA-TENG under 2.5 Hz vibration, the average output power with an external load of 20 M Ω reaches a steady state when the interval approaches 30 s. Considering that 3.5 Hz and 2.5 Hz are the lowest ambient vibration frequency to generate notable electricity from SR-TENG and MA-TENG respectively, it is adequate to choose the 30-seconds length for Δt in calculating the average power

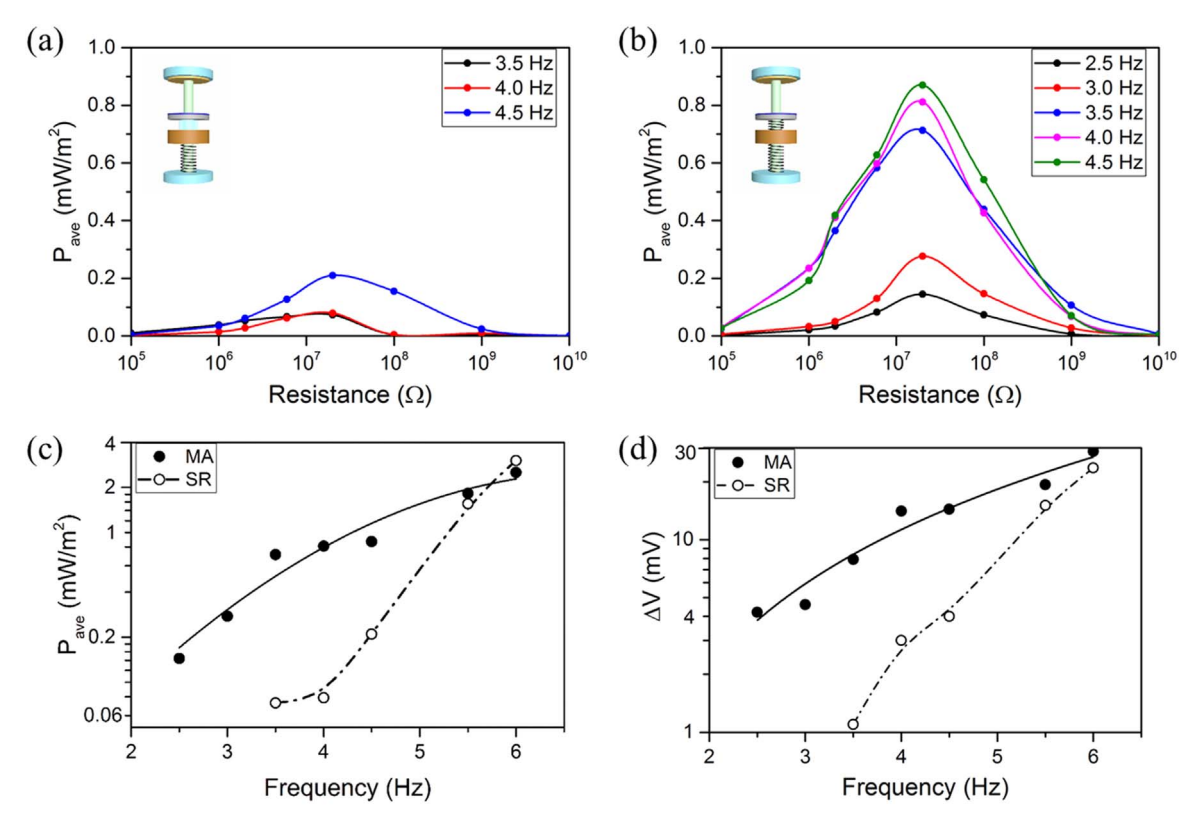


Fig. 5. Average output power of (a) SR-TENG and (b) MA-TENG with different load resistance operating at different vibration frequency lower than 5.0 Hz. (c) Comparison of maximum output power of MA-TENG and SR-TENG at different frequencies. (d) Voltage increase of a 0.33 mF capacitor after being charged for 30 s by MA-TENG and SR-TENG operating at different frequencies.

when the TENGs are connected to various external loads under different vibration frequency.

The average output power of SR-TENG and MA-TENG under ambient vibration with frequency lower than 5.0 Hz is presented in Fig. 5 while those with frequency higher than 5.0 Hz in Fig. S3 since they have different order of magnitude. Both TENGs exhibit maximum average output power when the external load resistance is around 20 M Ω , which is independent of the ambient vibration frequency. The strong comparison of the plots in Fig. 4(a) and (b) shows that MA-TENG starts to function as an electricity generator at a lower frequency and its output is much higher than the conventional SR-TENG at the same low frequency. Meanwhile, when the frequency is higher than 5.0 Hz, the maximum output power of both TENGs, as shown in Fig. S3, is about the same. It can be explained by the fact observed during experiment that the mass m_0 in SR-TENG and m_1 in MA-TENG could easily reach the top base at the same frequency as the ambient one even without velocity amplification when the vibration frequency was above 5.0 Hz. In such a case, although the collision between m_1 and m_2 brings a larger count of contact between the triboelectric layers as shown in Fig. 3, the major output contribution is attributed to the more intimate contact induced when the big masses m_0 and m_1 hit the top, as evidenced by the abrupt increase of output of both TENGs when the frequency changes from under 5.0 Hz to above 5.0 Hz. The maximum output power of both TENGs under different ambient vibration frequencies is summarized in Fig. 5(c), which clearly shows the enhanced performance of MA-TENG at low vibration frequency, with a maximum power ratio of 10:1 at 4.0 Hz. One point worth mentioning is that the structure of the TENGs, such as mass weight, springs, device height and etc, were not optimized in this work, and thus it is the relative comparison of their output power, rather than the absolute values, that is the focus of discussion. To further validate the results, the TENGs were used to charge a 0.33 mF capacitor at different vibration frequencies and the voltage increase of the capacitor after

30 s charging is plotted in Fig. 5(d). The comparison trend is highly consistent with that in Fig. 5(c), demonstrating the performance enhancement of MA-TENG in practical application. Considering that no other changes necessary in the device structure or operating mode, therefore, introducing a mechanical amplifier into TENG by splitting one single mass into two masses of large weight ratio is a simple but effective way to enhance its electrical output especially at low vibration frequency.

5. Conclusion

In summary, a MA-TENG with amplified frequency and displacement is designed based on velocity amplification using coupled-springs in order to improve its output performance under low-frequency vibration. To quantitatively compare their performance, a new scheme of comparing different TENGs using average output power is proposed and the process of choosing the appropriate time interval for analysis is demonstrated. The scheme takes into account the temporal variation in electrical output and offers a more accurate and convincing evaluation of TENG performance compared to previously used instantaneous power, especially in the case with infrequent or irregular mechanical input. It can serve as a standard for evaluating and comparing TENGs with different structures and operating modes in practical working environment, where the vibration is not periodic as in laboratory simulation. The corresponding analysis based on experimental results demonstrates a performance boost of the MA-TENG up to 10 times, which is further validated by the capacitor charging rate. This work serves as an important progress for the future development and application of TENG, especially for harvesting low-frequency vibration energy as well as the great prospect of blue energy.

6. Experimental methods

6.1. Fabrication of the TENGs

The bases, the shaft and three masses $(m_0, m_1 \text{ and } m_2)$ in SR-TENG and MA-TENG were designed using SolidWorks. The detailed dimensions of m_1 and m_2 are shown in Fig. S1. m_1 (55.91 g) is made of brass, with a diameter of 1 in. and a height of 0.5 in.; m_2 (4.28 g) is made of aluminum, with a diameter of 1 in. and a height of 0.1 in. m_0 (60.87 g) is made by binding together m_1 and m_2 with a lightweight acrylic rim to achieve a similar total weight $(m_0 \sim m_1 + m_2)$. The long spring attached to m_0 and m_1 has a length of 0.75 in. and a spring constant of 2.5 lbs./ inch; the short spring on m_2 has a length of 0.25 in. and a spring constant of 13.5 lbs./inch. The steel shaft has a diameter of 1/8 in. and a length of 3 in.. The PTFE film was pasted onto m_0 or m_2 with foam tape and the copper film was attached to the top base using insulating Kapton tape.

6.2. Vibration testing of the TENGs

The vibration at different frequencies was stimulated using a shaker (ET-126B Electrodynamic Transducer, Labworks Inc.). The shaker was controlled using a sine servo controller (SC-121, Labworks Inc.) and a linear power amplifier (PA-151, Labworks Inc.). The acceleration rate and vibration amplitude of the shaker at different frequency were recorded in Table SI. The short-circuit current of both TENGs was measured using a Keithley 6514 system electrometer, while the output voltage and transferred charge with different load resistance were measured by two electrometers simultaneously. The whole metal bases were grounded during measurement.

Acknowledgements

C. W. and R.L contributed equally to this work. This research was supported by the Hightower Chair foundation, the 'thousands talents' program for pioneer researcher and his innovation team and National Natural Science Foundation of China (Grant no. 51432005).

Appendix A. Supplementary material

Supplementary data associated with this article can be found in the online version at http://dx.doi.org/10.1016/j.nanoen.2016.12.061.

References

- F.-R. Fan, Z.-Q. Tian, Z. Lin Wang, Flexible triboelectric generator, Nano Energy 1 (2012) 328–334.
- [2] Z.L. Wang, Triboelectric nanogenerators as new energy technology and self-powered sensors principles, problems and perspectives, Faraday Discuss 176 (2014) 447–458.
- [3] Z.L. Wang, J. Chen, L. Lin, Progress in triboelectric nanogenerators as a new energy technology and self-powered sensors, Energy Environ. Sci. 8 (2015) 2250–2282.
- [4] R. Hinchet, W. Seung, S.-W. Kim, Recent progress on flexible triboelectric nanogenerators for selfpowered electronics, ChemSusChem 8 (2015) 2327–2344.
- [5] J. Chen, Y. Huang, N. Zhang, H. Zou, R. Liu, C. Tao, X. Fan, Z.L. Wang, Micro-cable structured textile for simultaneously harvesting solar and mechanical energy, Nat. Energy 1 (2016) 16138.
- [6] S. Niu, X. Wang, F. Yi, Y.S. Zhou, Z.L. Wang, A universal self-charging System driven by random biomechanical energy for sustainable operation of mobile electronics, Nat. Commun. 6 (2015) 8975.
- [7] K.N. Kim, J. Chun, J.W. Kim, K.Y. Lee, J.-U. Park, S.-W. Kim, Z.L. Wang, J.M. Baik, Highly stretchable 2D fabrics for wearable triboelectric nanogenerator under harsh environments, ACS Nano 9 (2015) 6394–6400.
- 8] U. Khan, S.-W. Kim, Triboelectric nanogenerators for blue energy harvesting, ACS

- Nano 10 (2016) 6429-6432.
- [9] M.-L. Seol, J.-H. Woo, S.-B. Jeon, D. Kim, S.-J. Park, J. Hur, Y.-K. Choi, Vertically stacked thin triboelectric nanogenerator for wind energy harvesting, Nano Energy 14 (2015) 201–208.
- [10] J. Wang, S. Li, F. Yi, Y. Zi, J. Lin, X. Wang, Y. Xu, Z.L. Wang, Sustainably powering wearable electronics solely by biomechanical energy, Nat. Commun. 7 (2016) 12744
- [11] C. Wu, X. Wang, L. Lin, H. Guo, Z.L. Wang, Paper-based triboelectric nanogenerators made of stretchable interlocking kirigami patterns, ACS Nano 10 (2016) 4652–4659.
- [12] L. Lin, Y. Xie, S. Wang, W. Wu, S. Niu, X. Wen, Z.L. Wang, Triboelectric active sensor array for self-powered static and dynamic pressure detection and tactile imaging, ACS Nano 7 (2013) 8266–8274.
- [13] D.Friedman, H.Heinrich, D.W.Duan, A low-power CMOS integrated circuit for field-powered radio frequency identification tags, in: Proceedings of the 1997 IEEE International Solid-State Circuits Conference. Digest of Technical Papers. 43rd ISSCC., 1997, pp. 294–295.
- [14] M. Chinchilla, S. Arnaltes, J.C. Burgos, Control of permanent-magnet generators applied to variable-speed wind-energy systems connected to the grid, IEEE Trans. Energy Convers. 21 (2006) 130–135.
- [15] S. Rahman, Green power: what is it and where can we find it?, IEEE Power Energy Mag. 1 (2003) 30-37.
- [16] Y. Zi, H. Guo, Z. Wen, M.-H. Yeh, C. Hu, Z.L. Wang, Harvesting low-frequency (5 Hz) irregular mechanical energy: a possible killer application of triboelectric nanogenerator, ACS Nano 10 (2016) 4797–4805.
- [17] H.Kulah, K.Najafi, An electromagnetic micro power generator for low-frequency environmental vibrations, in: Proceedings of the 17th IEEE International Conference on. (MEMS), 2004, pp. 237–240.
- [18] H.-J.Jung, I.-H.Kim, D.Y.Min, S.-H.Sim, J.-H.Koo, A hybrid electromagnetic energy harvesting device for low frequency vibration, in: Proceedings of the SPIE 8688, Active and Passive Smart Structures and Integrated Systems, 2013, p. 86881I.
- [19] S.Palagummi, F.G.Yuan, A vibration energy harvester using diamagnetic levitation, in: Proceedings of the SPIE 8688, Active and Passive Smart Structures and Integrated Systems, 2013, p. 86880N.
- [20] J. Yang, J. Chen, Y. Yang, H. Zhang, W. Yang, P. Bai, Y. Su, Z.L. Wang, Broadband vibrational energy harvesting based on a triboelectric nanogenerator, Adv. Energy Mater. 4 (2014) 1301322.
- [21] J. Chen, G. Zhu, W. Yang, Q. Jing, P. Bai, Y. Yang, T.-C. Hou, Z.L. Wang, Harmonic-resonator-based triboelectric nanogenerator as a sustainable power source and a, Adv. Mater. 25 (2013) 6094–6099.
- [22] S. Wang, S. Niu, J. Yang, L. Lin, Z.L. Wang, Quantitative measurements of vibration amplitude using a contact-mode freestanding triboelectric nanogenerator, ACS Nano 8 (2014) 12004–12013
- [23] S.D. Moss, G.A. Hart, S.K. Burke, G.P. Carman, Hybrid rotary-translational vibration energy harvester using cycloidal motion as a mechanical amplifier, Appl. Phys. Lett. 104 (2014) 033506.
- [24] F. Cottone, R. Frizzell, S. Goyal, G. Kelly, J. Punch, Enhanced vibrational energy harvester based on velocity amplification, J. Intell. Mater. Syst. Struct. 25 (2014) 443–451.
- [25] Ö. Zorlu, E.T. Topal, H. Kulah, A vibration-based electromagnetic energy harvester using mechanical frequency Up-conversion method, IEEE Sens. J. 11 (2011) 481–488.
- [26] S. Ju, S.H. Chae, Y. Choi, S. Jun, S.M. Park, S. Lee, H.W. Lee, C.H. Ji, frequency Up-converted low frequency vibration energy harvester using trampoline effect, J. Phys.: Conf. Ser. 476 (2013) 012089.
- [27] B. Rodgers, S. Goyal, G. Kelly, M. Sheehy, The dynamics of multiple pair-wise collisions in a chain for designing optimal shock amplifiers, Shock Vib. 16 (2009) 99–116.
- [28] D. O'Donoghue, R. Frizzell, G. Kelly, K. Nolan, J. Punch, The influence of mass configurations on velocity amplified vibrational energy harvesters, Smart Mater. Struct. 25 (2016) 055012.
- [29] L. Lin, Y. Xie, S. Niu, S. Wang, P.-K. Yang, Z.L. Wang, Robust triboelectric nanogenerator based on rolling electrification and electrostatic induction at an instantaneous energy conversion efficiency of ~55%, ACS Nano 9 (2015) 922−930.
- [30] M. Kanik, M.G. Say, B. Daglar, A.F. Yavuz, M.H. Dolas, M.M. El-Ashry, M. Bayindir, A motion- and sound-activated, 3D-printed, chalcogenide-based triboelectric nanogenerator, Adv. Mater. 27 (2015) 2367–2376.
- [31] G. Zhu, J. Chen, T. Zhang, Q. Jing, Z.L. Wang, Radial-arrayed rotary electrification for high performance triboelectric generator, Nat. Commun. 5 (2014) 3426.
- [32] G. Cheng, Z.-H. Lin, L. Lin, Z.-l. Du, Z.-L. Wang, Pulsed nanogenerator with huge instantaneous output power density, ACS Nano 7 (2013) 7383–7391.
- [33] Y. Zi, S. Niu, J. Wang, Z. Wen, W. Tang, Z.L. Wang, Standards and figure-of-merits for quantifying the performance of triboelectric nanogenerators, Nat. Commun. 6 (2015) 8376.
- [34] Y. Zi, J. Wang, S. Wang, S. Li, Z. Wen, H. Guo, Z.L. Wang, Effective energy storage from a triboelectric nanogenerator, Nat. Commun. 7 (2016) 10987.